Aceh Int. J. Sci. Technol., 14(1) 23-42
April 2025
doi: 10.13170/aijst.14.1.45308

Aceh International Journal of Science and Technology
ISSN: p-2088-9860; e-2503-2398
Journal homepage: http://jurnal.usk.ac.id/aijst

Petrology and Geochemistry of Igneous Rocks in Gunung Badak Complex, Ciletuh Palabuhanratu Geopark, Sukabumi, West Java

Millati Amalia Sentosa[1*], Mega Fatimah Rosana[2], Cipta Endyana[3]

[1]Department of Geological Engineering, Faculty of Geological Engineering, Padjadjaran University, 40132, Indonesia

*Corresponding author: millati22001@mail.unpad.ac.id

Received : March 25, 2025
Received in revised from: May 23, 2025
Accepted : May 24, 2025
Online : June 4, 2025

Abstract – Gunung Badak Complex is located in Ciletuh Palabuhanratu UNESCO Global Geopark, which preserves significant records of tectonic evolution in Southern West Java. This research aims to characterize igneous rocks and interpret tectonic implications. The methodology includes petrographic analysis, major element geochemical characterization using X-Ray Fluorescence (XRF), and trace elements and Rare Earth Element (REE) analysis using Inductively Coupled Plasma Mass Spectrometry (ICP-MS) from 8 selected samples. The results identify three distinct rock groups consisting of diorite (SiO_2 51.5-52.48%), basalt (SiO_2 50.69-52.52%), and serpentinized peridotite (SiO_2 40.59%, MgO 34.63%). Diorite and basalt exhibit tholeiitic affinity with low K_2O (0.25-0.69%), Mg# 49.67-58.13, indicating early-stage island arc magmatism. Serpentinized peridotite exhibits residual harzburgite characteristics with Mg# 89.29. Trace element geochemistry shows enrichment of LILE (Cs, Ba, Pb, Sr) relative to HFSE (Nb, Zr), with negative Nb-Ta anomalies and La/Nb ratios of 2.21-3.75 typical of subduction environments. Diorite-basalt displays moderate LREE enrichment ($(La/Yb)_N$ 1.40-2.63), while serpentinized peridotite shows LREE depletion ($(La/Yb)_N$ 0.54). Dy/Yb ratios (1.20-1.91) indicate magma sources from partial melting of spinel peridotite at depths <50 km. The geodynamic model indicates that serpentinized peridotite originated from lithospheric mantle in a supra-subduction zone (SSZ) environment during Eocene subduction initiation, while diorite and basalt formed during early Miocene island arc magmatism (~22 Ma).

Keywords: igneous rock, Island Arc Tholeiitic (IAT), Supra-Subduction Zone (SSZ), tectonic implications, Gunung Badak

Introduction

Ciletuh Palabuhanratu UNESCO Global Geopark (CPUGGp) is located in Sukabumi Regency, West Java Province, and represents an area with unique and complex geological diversity that functions as a natural laboratory for geological studies (Hall *et al.*, 2007; Martodjojo *et al.*, 1977; Sukamto, 1975). One of the main geological phenomena in this area is the mélange complex, which consists of chaotically mixed rocks with heterogeneous composition (Martodjojo *et al.*, 1977; Sukamto, 1975). This makes Ciletuh one of the three locations on Java Island that expose Pre-Tertiary rocks, along with Luk Ulo in Kebumen, Central Java Province, and Jiwo Hills in Klaten, Central Java Province (van Bemmelen, 1949; Verbeek and Fennema, 1896).

The Ciletuh mélange complex, as shown in Figure 1, formed due to the collision between the Eurasian Plate and the Indo-Australian Plate during the Cretaceous Period, resulting in a mixture of various rock types including ultrabasic, metamorphic, deep-sea sediments, and continental sediments (Hamilton, 1979; Satyana *et al.*, 2021; Thayyib *et al.*, 1977). Gunung Badak, as part of CPUGGp, attracts attention due to the presence of igneous rocks within this mélange zone, including diorite intrusions located south of Gunung Badak (Rosana *et al.*, 2019; Satyana *et al.*, 2021).

Although CPUGGp has been internationally recognized and has become the focus of various geological studies, there is a significant knowledge gap regarding the petrological and geochemical characteristics of igneous

Aceh Int. J. Sci. Technol., 14(1) 23-42
April 2025
doi: 10.13170/aijst.14.1.45308

rocks in the Gunung Badak Complex, especially in relation to regional tectonic evolution. Previous studies have focused more on aspects of geological structure and regional tectonics, while the detailed characteristics of igneous rocks, petrogenesis, and their implications for West Java tectonics have not been comprehensively studied. This research aims to characterize the igneous rocks in the Gunung Badak Complex through petrological and geochemical analyses to understand rock petrogenesis and interpret their tectonic implications in the context of the regional geological evolution of West Java. The results are expected to enrich the understanding of the geoheritage of this area and support the development of education and geotourism in Ciletuh Palabuhanratu UNESCO Global Geopark (CPUGGp).

Geological Setting

Gunung Badak is located within the Ciletuh Mélange Complex in Ciemas District, West Java Province, which formed due to tectonic activity and subduction processes that have been ongoing since the Pre-Tertiary. This area is situated at the southwestern tip of Java Island, influenced by the interaction between the Indo-Australian and Eurasian Plates. This subduction zone triggers volcanism, tectonic deformation, and the formation of ophiolitic rocks in West Java(Hall, 2007; Hamilton, 1979; Katili, 1975).

According to (Satyana *et al*., 2021), Ciletuh is believed to have formed from the subduction of the Proto-Indian plate beneath the Sundaland Block during the Early-Late Eocene (55.3-37.8 Ma), which differs from the Cretaceous subduction in Luk Ulo, Central Java and Meratus, South Kalimantan. This process illustrates the different subduction dynamics along the Sundaland margin from the Mesozoic to the Cenozoic, accompanied by plate rollback and formation of mélange complexes with metamorphic rocks (greenschist) as the main component, formed in a shallow subduction environment (Hardiyono *et al*., 2022; Satyana *et al*., 2021).

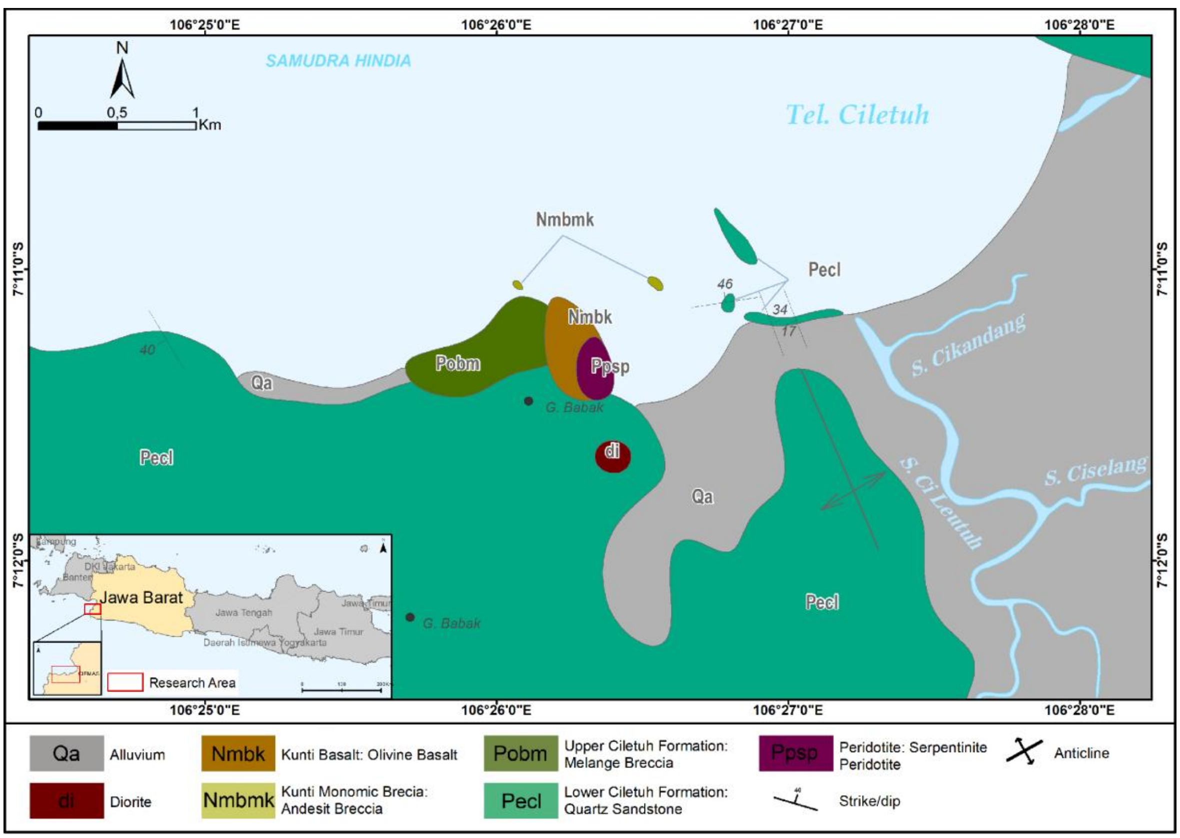

Figure 1. Simplified geological map of the study area (modified after Rosana *et al*., 2019).

The Ciletuh Complex developed in a supra-subduction zone (SSZ) environment, where ophiolites formed through the rollback process of an old subduction plate (Jurassic Woyla slab) beneath the Proto-Indian oceanic crust (Satyana *et al*., 2021). This mechanism caused rifting on the overriding plate and the formation of ophiolites with island arc tholeiitic (IAT) characteristics. Serpentinized peridotite (Ppsp) in Gunung Badak represents mantle fragments altered by subduction fluids, with mesh and bastite textures resulting from hydration of olivine and pyroxene (Rosana *et al*., 2019). This serpentinization process is related to the dehydration of the subduction plate at depths of 10-25 km (zeolite-greenschist facies), consistent with the absence of high-pressure metamorphic rocks (blueschist/eclogite) in Ciletuh (Satyana *et al*., 2021). K-Ar analysis of greenschist (chlorite-muscovite) in Pasir Luhur yielded ages of 55.2-37.8 Ma (Early-Late Eocene), confirming the time of active subduction (Ikhram *et al*., 2023; Satyana *et al*., 2021).

The presence of basaltic pillow lava in Gunung Badak indicates submarine volcanic activity that has a closer relationship with Jampang volcanism in the Miocene compared to the formation of Ciletuh ophiolites (Satyana *et al*., 2021). K-Ar analysis of this pillow lava shows an age of approximately 22.4 million years (Early Miocene), with calc-alkaline characteristics and island arc tholeiitic (IAT) affinities, indicating formation in a subduction-related volcanic environment (Hardiyono *et al*., 2022). Mapping conducted by (Rosana *et al*., 2019) on the Cikadal-Lengkong Sheet (Figure 1), particularly in Gunung Badak, shows the distribution of mélange rocks (Ppsp), Miocene volcanic rocks (Nmbk), and diorite intrusions (Di). The diorite intrusion south of Gunung Badak (Figure 1) is part of the Early Miocene Jampang volcanism. The presence of Upper Early Miocene diorite shows a post-subduction magmatism phase that overlaps with the Eocene mélange complex. This research requires K-Ar dating to determine the age of diorite and serpentinized peridotite rocks more clearly, considering that only basaltic rocks in this area have geochronological data from the study by (Hardiyono *et al*., 2022).

Recent analyses show that Ciletuh subduction occurred in the Eocene, not the Cretaceous as previously thought. This process involved the formation of ophiolites and metamorphic rocks in a supra-subduction zone environment (Satyana *et al*., 2021). Nevertheless, the magmatic evolution and its relationship with regional tectonics are still not fully understood. Gunung Badak represents a complex geological region formed from continuous tectonic activity since the Pre-Tertiary, showing complex interactions between subduction processes and Miocene magmatic activity in West Java.

Materials and Methods

This research combines field and laboratory analyses to examine the petrological and geochemical characteristics of igneous rocks in Gunung Badak, Ciemas District, Ciletuh Palabuhanratu UNESCO Global Geopark. From field observations, 11 fresh rock samples (Figure 2 and 3) with minimal alteration were selected for petrographic analysis, and from that number, 8 samples were selected for further geochemical analysis (Table 1). Samples were representatively selected including 5 diorites, 2 basalts, and 1 serpentinized peridotite. Petrographic analysis was conducted at the Petrology and Mineralogy Laboratory, Padjadjaran University, to identify minerals and rock textures to understand magmatic processes and rock formation conditions.

Geochemical characterization was conducted at the Intertek Laboratory, Jakarta, using two methods comprising X-ray Fluorescence (XRF) to identify major elements (SiO_2, TiO_2, Al_2O_3, and others) in weight percent concentration, and Inductively Coupled Plasma Mass Spectrometry (ICP-MS) for trace elements and rare earth elements (REE) analysis with high accuracy, allowing detection down to parts per million (ppm) levels. This data is important for interpreting tectonic environments and rock formation processes, as well as providing deeper information about magma sources and geochemical conditions that influenced the formation of these rocks (Gill, 2010; Wilson, 1989). Our findings were corroborated through comparison with existing literature, enhancing understanding of Ciletuh's geotectonic and magmatic chronology. This interpretation synthesizes key perspectives from multiple researchers (Bhat *et al*., 2019; Escuder Viruete *et al*., 2006; Hardiyono *et al*., 2022; Shervais, 2008; Torró *et al*., 2017; Wu *et al*., 2019; Yin *et al*., 2010).

Results and Analysis

Rock types and Petrography

Microscopic analysis reveals that the igneous rocks of the Gunung Badak Complex exhibit significant variations in mineral composition and texture (Figure 4). Based on petrographic characteristics, the investigated rocks are classified into three main groups consisting of intermediate rocks (diorite intrusion), mafic rocks (basalt lava), and ultramafic rocks (serpentinized peridotite).

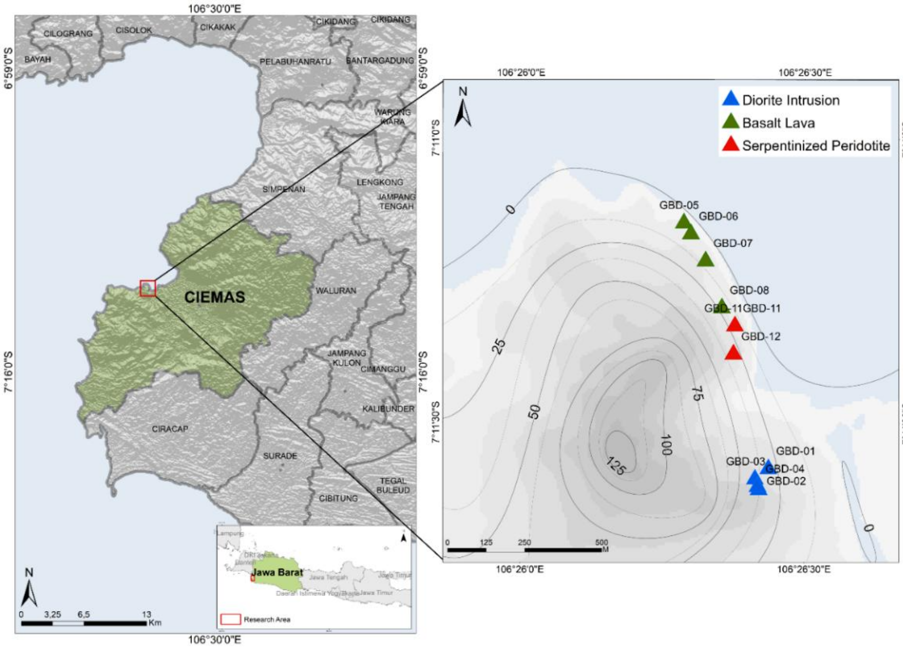

Figure 2. Maps showing localities of igneous rock samples analyzed in this study.

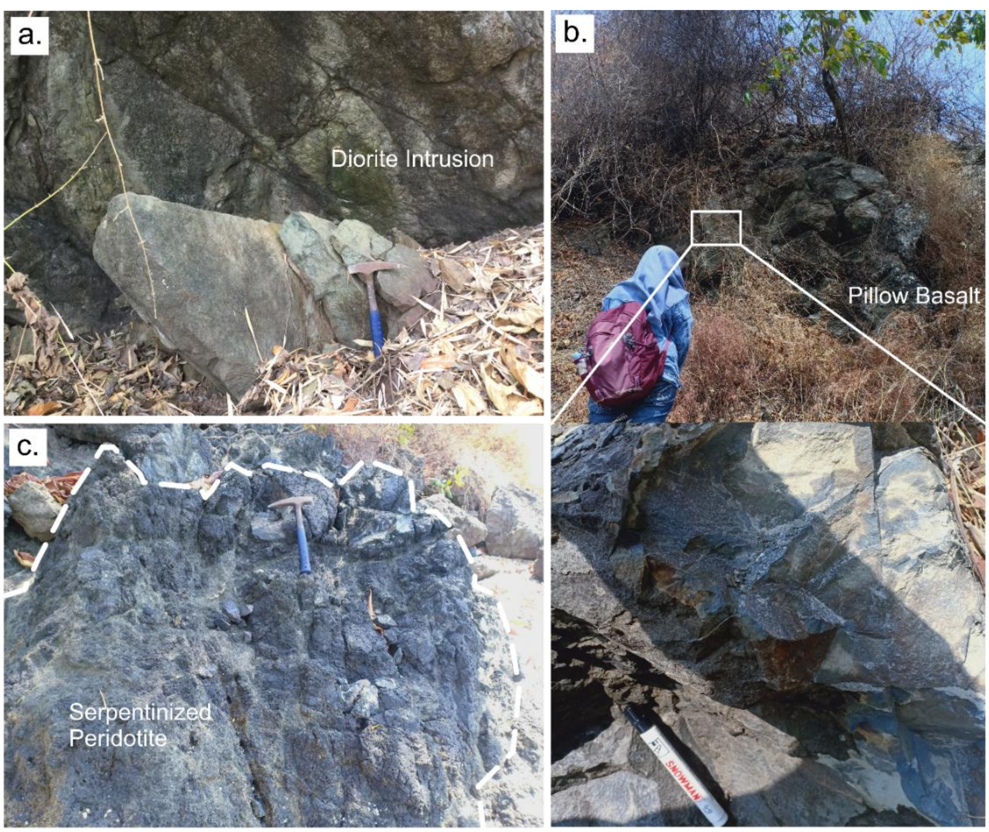

Figure 3. Field photographs showing the various lithologies in Gunung Badak (a) Diorite intrusion; (b) Basalt lava with pillow structure; (c) Serpentinized Peridotite.

doi: 10.13170/aijst.14.1.45308

Diorite Intrusion

Diorite samples (GBD01–GBD04 and GBD11) represent intermediate rocks with porphyritic texture, displaying holocrystalline and hypidiomorphic granular characteristics. Phenocrysts measuring 0.8-2.5 mm are dominated by plagioclase (41-70%) and pyroxene embedded in a fine to medium-grained phaneritic groundmass (0.1-0.5 mm). Plagioclase is present as oligoclase to andesine ($An_{24\text{-}36}$) exhibiting albite and carlsbad-albite twinning, commonly showing sieve texture and undergoing alteration to clay minerals (1-3%), chlorite (7-22%), and sericite (1-3%). The plagioclase sieve texture indicates thermal disequilibrium or magma mixing during crystallization. The pyroxene component consists of clinopyroxene (2-21%, 0.5-1.8 mm) in the form of augite with wavy extinction and diopside displaying twinning, as well as orthopyroxene (1-4%, 0.3-1.2 mm) of hypersthene type exhibiting oscillatory zoning patterns and sieve texture in pseudomorphs. K-feldspar (3-6%, 0.4-1.5 mm) appears as orthoclase with Carlsbad twinning. Glomeroporphyritic texture comprising plagioclase and pyroxene aggregates (1.5-3.0 mm) is commonly observed. Opaque minerals (3-8%, <0.3 mm) are evenly distributed throughout the rock. Sample GBD11 exhibits more intensive alteration with plagioclase and K-feldspar partially replaced by calcite (4%) and epidote (1%), as well as chlorite displaying anomalous interference.

Basalt Lava

Basalt samples (GBD05–GBD07, and GBD10) are hypocrystalline mafic rocks characterized by porphyritic texture with intergranular-intersertal groundmass. Phenocrysts measuring 0.6-2.0 mm consist of plagioclase (33-49%) of oligoclase type ($An_{24\text{-}30}$), pyroxene, and K-feldspar embedded in a groundmass of feldspar microlites (0.05-0.3 mm), pyroxene, opaque minerals (4-7%), and volcanic glass (12-24%). The significant presence of volcanic glass indicates relatively rapid cooling. Plagioclase displays zonation, albite-carlsbad twinning, and fine-coarse sieve texture with albitization features. Albitization phenomena likely cause the transformation of plagioclase from basic (Ca) to more acidic (Na), thereby affecting the reduction of the anorthite component. Plagioclase content is higher in GBD05 and GBD07 (46-49%) compared to GBD06 and GBD10 (33-34%). Mafic minerals are dominated by clinopyroxene (13-16%) of diopside-augite type with twin structures and wavy extinction (hourglass structure), accompanied by minor orthopyroxene (1-2%) of hypersthene type. K-feldspar (4-5%) is present as sanidine with Carlsbad twinning. Cumulophyric and vesicular amygdaloidal textures are commonly encountered. Weak to moderate alteration is marked by the presence of clay minerals (2-10%) and chlorite (3-10%), partly forming veins that cut across the thin section.

Serpentinized Peridotite

Serpentinized peridotite (GBD09 and GBD12) represents tectonic ultramafic rocks with varying textures. GBD09 exhibits holocrystalline inequigranular porphyroclastic texture (Mercier and Nicolas, 1975) of ophiolite tectonics (Marchesi *et al*., 2009), while GBD12 shows holocrystalline equigranular texture. Both samples form sea and island patterns. Primary minerals consist of relict olivine (31-34%) with somewhat rounded form exhibiting mesh texture, orthopyroxene (20-24%) of enstatite type present as porphyroclasts reaching 3 mm displaying bastite texture, and minor clinopyroxene (2%) of diopside type. Evidence of ductile deformation is observed through undulatory extinction and kink bands in olivine and orthopyroxene, as reported in other residual mantle peridotites (Dupuis *et al*., 2005; Gu *et al*., 2016; Zhao *et al*., 2019). Thin exsolution lamellae of clinopyroxene in orthopyroxene indicate complex cooling of these rocks. Intensive serpentinization is marked by the presence of chrysotile (4-12%), lizardite (9-13%), and antigorite (11-22%) replacing primary minerals, and exhibiting mesh, hourglass, and bastite pseudomorph textures. Spinel (1%) is found as holly-leaf spinel maintaining its original composition due to its stability against serpentinization (Ahmed *et al*., 2005; Hellebrand *et al*., 2002). Magnetite (5-8%) fills fractures forming veins with higher content in GBD09, indicating more intense serpentinization compared to GBD12. The presence of garnet (<1%) in GBD09 suggests possible high-pressure metamorphism. Serpentine-filled fractures indicate that these rocks have experienced high pressure and friction during exhumation or obduction processes.

The petrographic characteristics of the three rock groups demonstrate complex magmatic evolution in the study area. Porphyritic diorite represents intermediate magmatism, basalt reflects rapid cooling of mafic magma, and serpentinized peridotite indicates the exposure of deformed mantle rocks. This association provides important clues regarding the tectonic setting and geodynamic evolution of the region.

doi: 10.13170/aijst.14.1.45308

Table 1. Petrographic characteristics of the investigated samples

Sample	Primary minerals	Secondary minerals	Texture	Rock type (Travis, 1955)	Rock type (Streckeisen, 1973, 1976)
GBD-01	Pl, Cpx, Opx, Kfs, Op	Clay, Chl	Porphyritic	Diorite porphyry	Diorite
GBD-02	Pl, Cpx, Kfs, Op	Clay, Chl, Ser			
GBD-03	Pl, Cpx. Kfs. Op	Clay, Chl			
GBD-04	Pl, Cpx, Opx, Kfs, Op	Clay, Chl, Ser			
GBD-11	Pl, Opx, Cpx, Hbl, Kfs, Op	Clay, Chl, Ser, Cal, Ep			
GBD-05	Pl, Cpx, Opx, Kfs, Op, Gl	Clay, Chl	Porphyritic intergranular-intersertal	Basalt porphyry	Basalt
GBD-06	Pl, Cpx, Opx, Kfs, Op, Gl	Clay, Chl			
GBD-07	Pl, Cpx, Opx, Kfs, Op, Gl	Clay, Chl			
GBD-10	Pl, Cpx, Opx, Kfs, Op, Gl	Clay, Chl			
GBD-09	Ol, Opx, Cpx	Ctl, Lz, Atg, Sp, Mgt	Holocrystalline	Peridotite	Harzburgite
GBD-12	Ol, Opx, Cpx	Ctl, Lz, Atg, Sp, Mgt, Brc	Holocrystalline		

*Sample numbers in italics are selected for geochemical analysis. Abbreviations for minerals: Pl, Plagioclase; Ol, Olivine; Opx, Orthopyroxene; Cpx, Clinopyroxene; Kfs, K-feldspar; Op, Opaque; Hbl, Hornblende; Gl, Glass; Sp, Spinel; Chl, Chlorite; Mgt, Magnetite; Atg, Antigorite; Cry, Chrysotile; Lz, Lizardite; Brc, Brucite; Ser, Sericite; Ep, Epidote.

Whole-rock geochemistry

Major elements

The major element analysis results (Table 2) demonstrate compositional differences reflecting various petrogenetic processes. LOI values vary (2.7-9.78%), with lower values in diorite and basalt (2.7-4.24%) indicating moderate alteration, while higher values in serpentinized peridotite (9.78%) suggest intensive serpentinization, consistent with petrographic observations.

In the TAS (Total Alkali-Silica) classification, diorite plots as monzodiorite, basalt as basaltic trachyandesite, while serpentinized peridotite plots as harzburgite in the ternary SiO_2-FeO*-MgO diagram (Figure 5a-b). All samples, except serpentinized peridotite, display calc-alkaline series (Figure 5d) with low-k (tholeiitic) content (Figure 5e, f), characterizing the early to intermediate stages of volcanic arc evolution. The linear trend in Harker diagrams for SiO_2 (50.69-52.52 wt%) in basalt and diorite indicates derivation from the same parent magma through limited differentiation. The decreasing patterns of MgO, FeOt, CaO, and TiO_2 with increasing SiO_2 (Figure 6), accompanied by increases in K_2O and Na_2O, reflect fractionation of mafic minerals (olivine, pyroxene) and accumulation of alkaline components in the residual magma. In contrast, serpentinized peridotite (SiO_2 40.59 wt%) shows significantly different composition, indicating a distinct origin and formation process from the diorite-basalt. The low TiO_2 content (<1.3%) in all samples indicates formation through subduction (orogenic) processes (Gill, 1981).

Trace and Rare Earth Element (REE)

Trace Elements

Rock samples show variation in trace element content corresponding to their rock types (Table 3). Diorite-basalt contains relatively low transitional elements (Ni 13-35 ppm, Cr 17-82 ppm, Co 27-33 ppm), while serpentinized peridotite is enriched in transitional elements (Ni 1670 ppm, Cr 1740 ppm, Co 99 ppm) reflecting mantle origin. The Ni and Cr content in peridotite exceeds primitive mantle values (Ni > 400 ppm and Cr > 800 ppm), indicating derivation from highly depleted mantle material (Saha *et al.*, 2018).

Aceh Int. J. Sci. Technol., 14(1) 23-42
April 2025
doi: 10.13170/aijst.14.1.45308

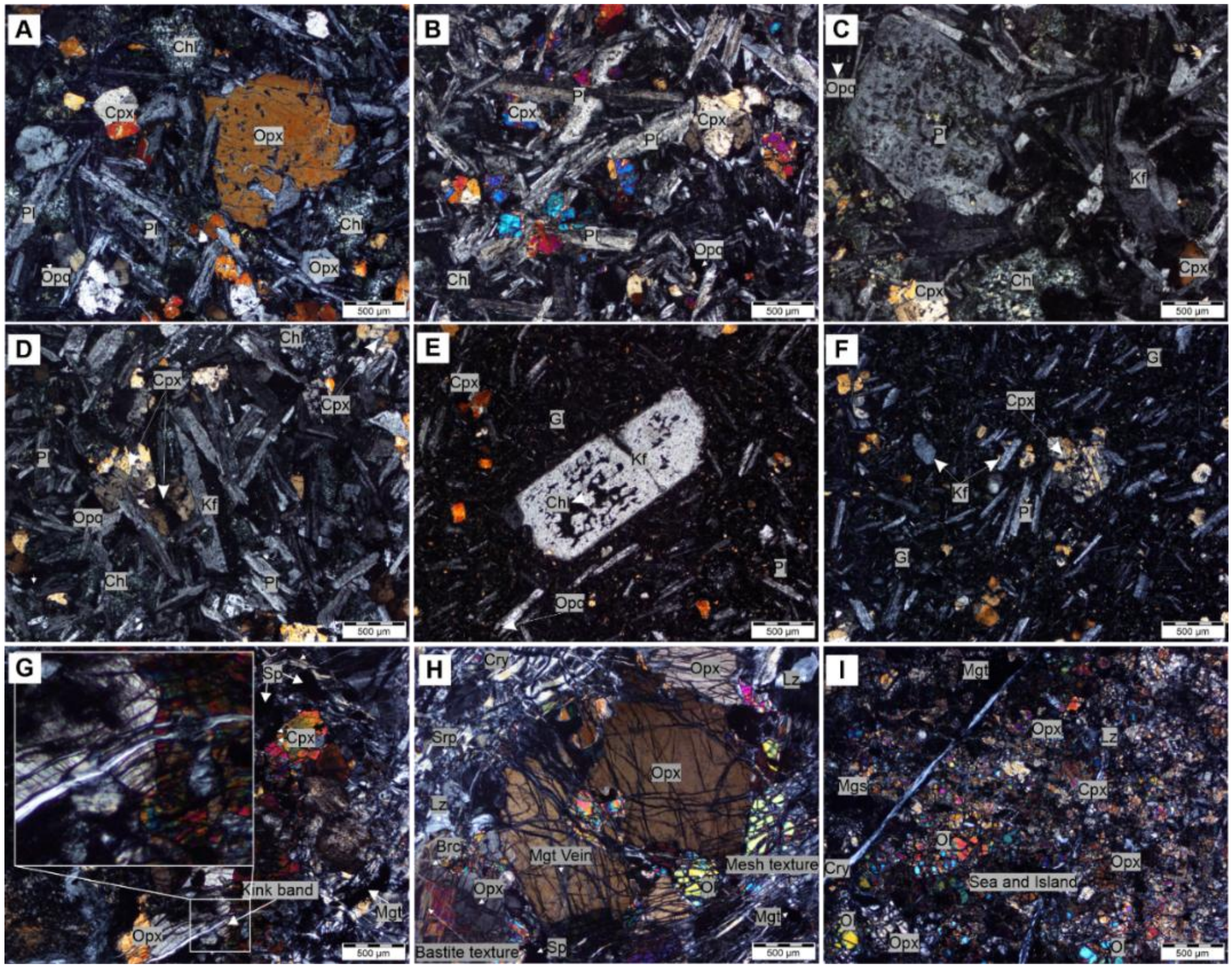

Figure 4. Photomicrographs of representative igneous rocks from Gunung Badak under cross-polarized light. (a) Orthopyroxene phenocrysts with plagioclase inclusions exhibits a sieve texture. (b) Altered plagioclase in a glomerocryst texture composed of plagioclase and pyroxene minerals (c) Coarse sieve texture in plagioclase phenocrysts altered by chlorite (d) Clinopyroxene and K-feldspar (orthoclase) exhibit a glomerocryst texture. (a-d) mineral assemblages shows porphyritic texture in cross-polarized light (e) Porphyritic texture with plagioclase as phenocrysts and chlorite inclusions within a coarse sieve texture. (f) Clinopyroxene exhibits twinning and microphenocrysts consist of plagioclase and pyroxene. (e and f) Intersertal texture can be observed in the occurrence of plagioclase, clinopyroxene, glass and opaque minerals. (g) Orthopyroxene and clinopyroxene show kink band textures due to ductile deformation. Part of the mineral shows altered and oxidized serpentine after olivine (h) Orthopyroxene is crosscut by magnetite veins and is surrounded by mafic minerals, part of which have been altered into serpentine. (i) Fibrous vein and mineral assemblages within mesh texture. Ol: Olivine, Opx: Orthopyroxene, Cpx: Clinopyroxene, Gl: Glass, Chl: Chlorite, Mgt: Magnesite, Atg: Antigorite, Cry: Chrysotile, Lz: Lizardite, Sp: Spinel, Brc: Brucite, Mgs: Magnesite, Ser: Sericite.

Geochemical patterns in the samples exhibit characteristic subduction environment features with relative enrichment of Large Ion Lithophile Elements (LILE) such as Cs, Ba, Pb, Sr compared to High Field Strength Elements (HFSE) such as Nb, Ta, Zr, Hf, and Ti, showing distinct negative Nb-Ta anomalies (Figure 9a, c, e). Most samples display Nb-Ta depletion patterns characteristic of island arc tholeiitic environments (Figure 8a, b), while serpentinized peridotite exhibits typical suprasubduction zone (SSZ) patterns. The high LILE/HFSE ratios and significant positive Pb anomaly indicate subduction influence in magma petrogenesis, supported by La/Nb (2.21-3.75) and Nb/Zr (0.02-0.05) ratios reflecting magmatic characteristics derived from interaction between slab fluids and subduction mantle peridotite (Green, 2006).

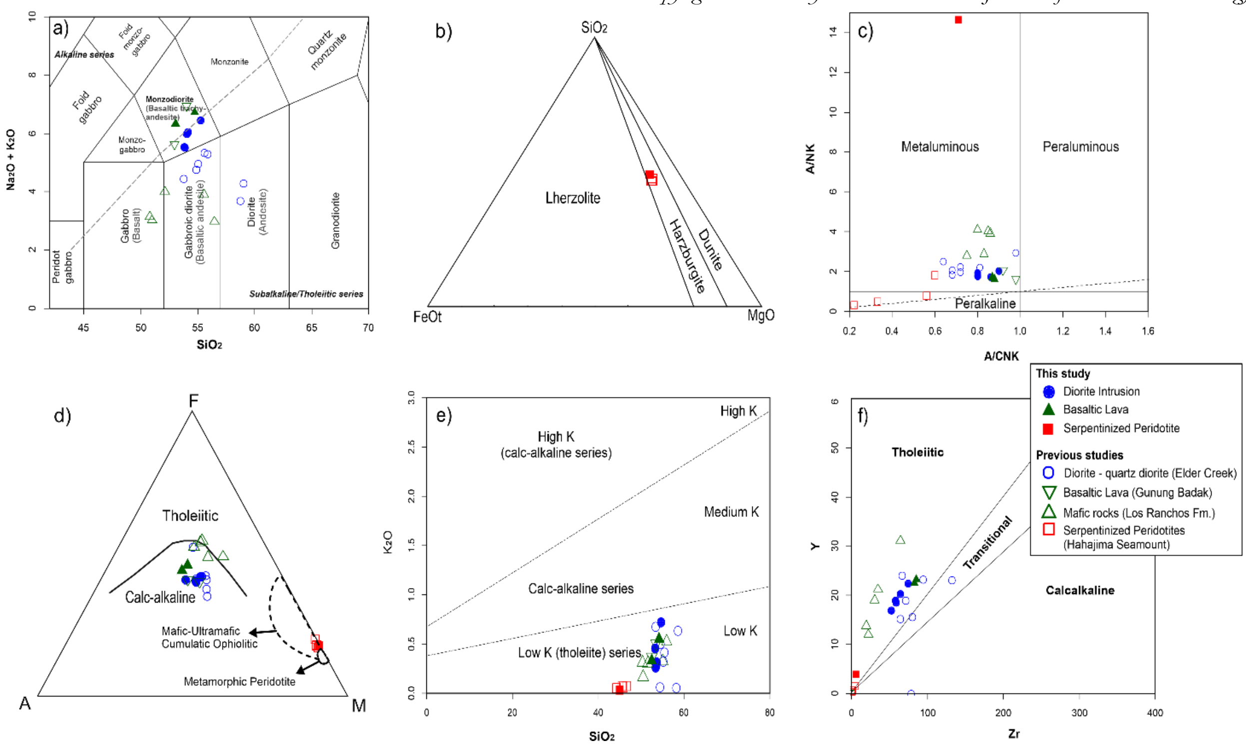

Figure 5. Magma types of Gunung Badak igneous rocks. (a) Na_2O+K_2O vs. SiO_2 diagram (Middlemost, 1994); (b) Triangular diagram of SiO_2-FeO*-MgO and fields (Pfeifer, 1979); (c) A/NK vs. A/CNK (Barret and MacLean, 1994; Shand, 1943). (d) AFM ternary diagram, the trend of the differentiation of tholeiitic and calc-alkaline magmas (Irvine and Baragar, 1971), the field of ultramafic cumulate and metamorphic peridotite (Coleman, 1977); (e) K2O vs. SiO_2 diagram (Le Maitre *et al*., 1989). (f) Zr vs. Y diagram (Barret and MacLean, 1994).

Table 2. Major element compositions and CIPW (Cross, Iddings, Pirsson, Washington) normative mineral percentages of Gunung Badak rocks.

Sample	Intermediate					Mafic		Ultramafic
	GBD-01	**GBD-02**	**GBD-03**	**GBD-04**	**GBD-11**	**GBD-05**	**GBD-07**	**GBD-09**
Lithology (Middlemost, 1994)	**Monzodiorite**	**Monzodiorite**	**Monzodiorite**	**Monzodiorite**	**Monzodiorite**	**Basaltic Tracy-andesite**	**Basaltic Tracy-andesite**	**N/A**
Major Element (XRF, wt.%)								
SiO_2	52.03	51.92	51.93	51.5	52.48	50.69	52.52	40.59
TiO_2	0.94	1	0.9	0.96	0.97	1.3	1.2	0.13
Al_2O_3	16.73	17.26	16.63	16.5	16.65	16.74	16.6	3.47
Fe2O3	9.07	9.48	8.91	9.25	8.78	10.81	10.05	8.23
MnO	0.15	0.15	0.15	0.16	0.18	0.18	0.15	0.11
MgO	6.14	6.43	6.24	6.26	5.32	5.39	5.07	34.63
CaO	6.32	5.83	6.2	6.6	5.26	5.25	4.71	2.54
Na2O	5.51	4.92	5.52	5.03	5.44	5.73	5.92	0.13
K2O	0.27	0.44	0.3	0.25	0.69	0.32	0.53	0.03
P2O5	0.111	0.128	0.112	0.113	0.203	0.262	0.259	0.01
LOI	2.99	2.7	3.6	3.46	4.24	3.35	3.23	9.78
Total	100,261	100,258	100,492	100,083	100,213	100,022	100,239	99,65
Mg#	57,29	57,35	58,13	57,29	54,54	49,67	50,00	89,29
CIPW Norms								
Quartz (Q)	0,00	0,75	0,00	0,23	0,75	0,00	0,05	0,00
Albite (Ab)	47,90	42,64	48,15	44,00	47,92	50,10	51,60	1,22
Anorthite (An)	20,63	24,21	20,24	22,38	19,70	19,62	17,65	9,73

doi: 10.13170/aijst.14.1.45308

Orthoclase (Or)	1,72	2,80	1,99	1,64	4,35	2,00	3,27	0,21
Diopside (Di)	6,37	1,35	6,56	6,41	2,70	1,53	0,89	3,24
Hypersthene (Hy)	8,52	15,77	7,71	13,15	12,54	8,43	12,60	32,88
Olivine (Ol)	2,97	0,00	3,69	0,00	0,00	3,32	0,00	42,85
Ilmenite (Il)	0,33	0,32	0,33	0,35	0,40	0,40	0,33	0,27
Magnetite (Mt)	0,00	0,00	0,00	0,00	0,00	0,00	0,00	0,25
Hematite (Hm)	9,32	9,71	9,18	9,56	9,14	11,17	10,35	8,94
Apatite (Ap)	0,27	0,31	0,27	0,28	0,50	0,64	0,63	0,03
Zircon (Zr)	0,01	0,01	0,01	0,01	0,01	0,02	0,02	0,00
Chromite (Cr)	0,02	0,02	0,02	0,01	0,02	0,00	0,00	0,37
Titanite (Tn)	1,95	2,09	1,85	1,98	1,96	2,78	2,61	0,00
Total	100	100	100	100	100	100	100	100

*LOI = Loss On Ignition

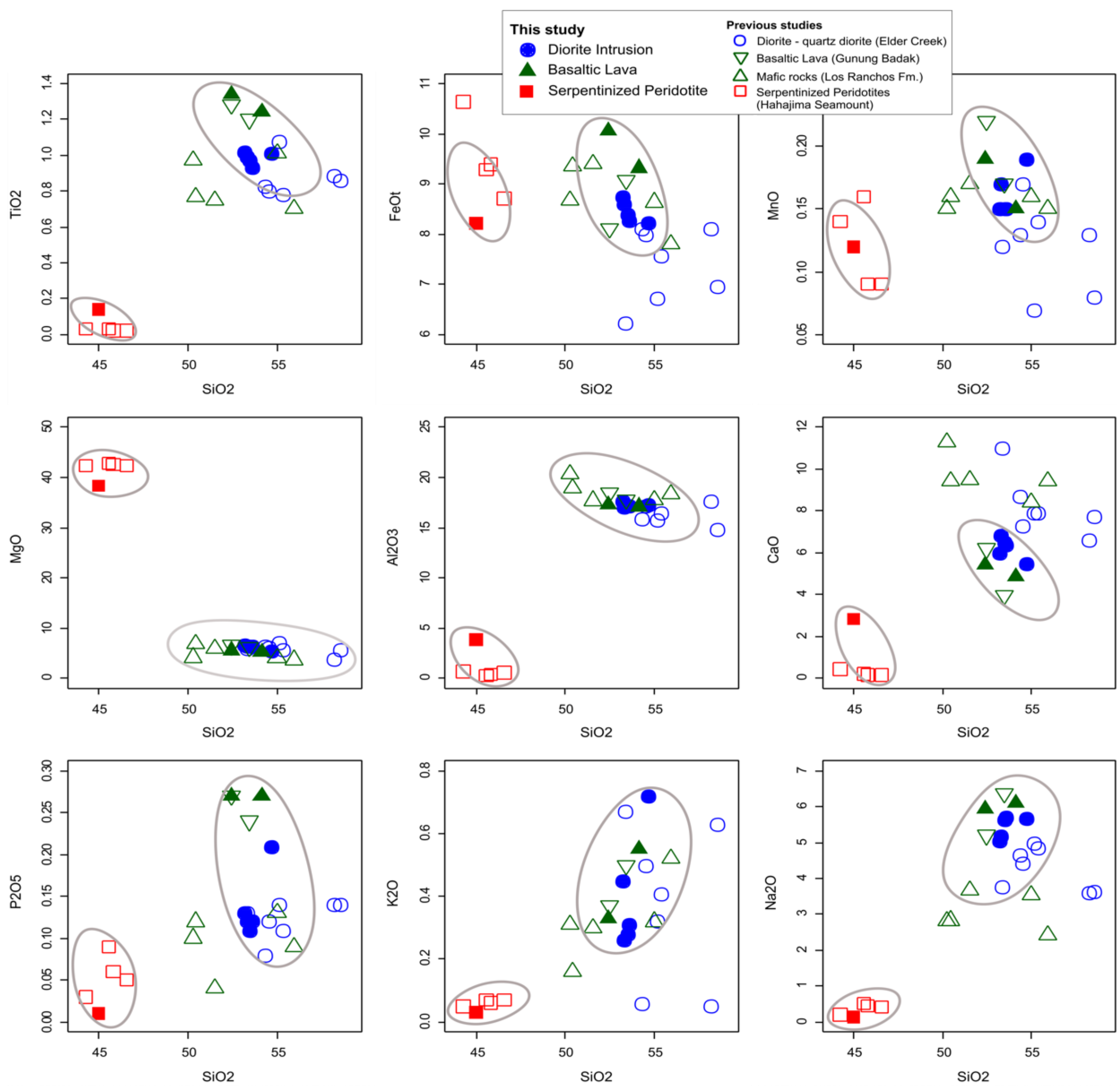

Figure 6. Harker variation diagrams showing major element oxides (wt.%) versus SiO_2 (wt.%) for samples from Gunung Badak.

Table 3. Trace element and REE compositions (ppm) of whole rock samples from Gunung Badak

Sample	GBD-01	GBD-02	GBD-03	GBD-04	GBD-11	GBD-05	GBD-07	GBD-09	N-type MORB	E-type MORB	OIB
Trace Element (XRF, ppm)											
Cs	4,3	0,5	0,1	0,05	0,3	4,1	3	0,05	0,01	0,06	0,39
Rb	3	4,8	2,9	2,3	11,2	5,2	12,3	2,2	0,56	5,04	31
Ba	191	339	401	282	263	117	118	39	6,30	57,00	350
Sr	356	506	1080	1070	529	1230	513	27,9	90,00	155,00	660
Pb	4	4	4	4	7	5	6	5	0,30	0,60	3,20
Th	0,49	0,56	0,53	0,56	1,45	1,29	1,34	0,09	0,12	0,60	4
U	0,15	0,21	0,18	0,16	0,37	0,4	0,48	0,025	0,05	0,18	1,02
Zr	52,3	64,2	58,7	57,3	73,8	85,2	83	5,6	74,00	73,00	280
Hf	1,5	1,8	1,8	1,6	2,6	2,4	2,2	0,2	2,05	2,03	7,80
Ta	0,08	0,08	0,07	0,07	0,15	0,23	0,22	0,025	0,13	0,47	2,70
Y	17	20,3	18,5	19	22,4	23,2	22,5	3,9	28,00	22,00	29
Nb	1,1	1,2	1,2	1,1	2,3	3,9	3,8	0,1	2,33	8,30	48
K	2040	3210	2260	1960	5210	2330	3970	160	600,00	2100,00	12000
Li	17,3	22	20,9	28,1	12,8	26	17,3	4	4,30	3,50	5,60
P	440	510	460	470	820	1060	1040	25	510,00	620,00	2700
Ti	5100	5360	5010	5560	5230	6990	6470	762	7600,00	6000,00	17200
Rare Earth Elements (ICP-MS, ppm)											
La	3,7	4,5	4,2	4	8,3	8,6	8,9	0,3	2,50	6,30	37
Ce	9,4	11,5	10,3	10,2	19,7	19,8	20	0,7	7,50	15,00	80
Pr	1,44	1,75	1,58	1,56	2,78	2,9	2,85	0,12	1,32	2,05	9,70
Nd	7,3	8,9	8,4	7,8	13,3	14,1	12,9	0,8	7,30	9,00	38,50
Sm	2,3	2,7	2,5	2,5	3,4	3,9	3,6	0,3	2,63	2,60	10
Eu	0,9	1	0,9	0,9	1,3	1,3	1,2	0,1	1,02	0,91	3
Gd	2,7	3,1	3,1	3	4	4,1	3,8	0,5	3,68	2,97	7,62
Tb	0,48	0,55	0,52	0,51	0,67	0,64	0,63	0,09	0,67	0,53	1,05
Dy	3,1	3,9	3,6	3,4	4,3	4,4	4,1	0,6	4,55	3,55	5,60
Ho	0,6	0,8	0,7	0,7	0,8	0,9	0,8	0,1	1,01	0,79	1,06
Er	1,9	2,2	2,3	2,1	2,6	2,5	2,4	0,4	2,97	2,31	2,62
Tm	0,3	0,3	0,3	0,3	0,3	0,4	0,4	0,05	0,46	0,36	0,35
Yb	1,9	2,2	2	1,9	2,3	2,3	2,6	0,5	3,05	2,37	2,16
Lu	0,28	0,34	0,3	0,28	0,37	0,35	0,35	0,06	0,46	0,35	0,30
Ratios											
ΣREE	36,3	43,74	40,7	39,15	64,12	66,19	64,53	4,62	39,12	49,09	198,96
Eu/Eu*	1,10	1,06	0,99	1,00	1,08	0,99	0,99	0,79	1,00	1,00	1,05
(La/Yb)N	1,40	1,47	1,51	1,43	2,65	2,63	2,36	0,54	0,59	1,91	12,29
Dy/Yb	1,63	1,77	1,80	1,79	1,87	1,91	1,58	1,20	1,49	1,50	2,59
La/Nb	3,36	3,75	3,50	3,64	3,61	2,21	2,34	3	1,07	0,76	0,77
Nb/Zr	0,02	0,02	0,02	0,02	0,03	0,05	0,05	0,02	0	0	0
Th/La	0,13	0,12	0,13	0,14	0,17	0,15	0,15	0,30	0,05	0,10	0,11

Rare Earth Elements (REE)

Rare earth elements distributions exhibit modest Eu anomalies (Eu/Eu* = 0,79-1,10), suggesting limited plagioclase segregation during magma evolution. Low Mg# values in diorite-basalt rocks (49.67-58.13) and high values in serpentinized peridotite (89.29), along with varying ΣREE content of 36.3-66.19 ppm (diorite-basalt) and 4.62 ppm (serpentinized peridotite), demonstrate differences in source and magmatic evolution processes.

REE patterns in diorite-basalt show moderate LREE (Light Rare Earth Elements) enrichment with (La/Yb)N 1.40-2.63 and flat HREE (Heavy Rare Earth Elements) patterns (Figure 9b, d), similar to E-MORB (Enriched Mid-Ocean Ridge Basalt) and IAT basalt patterns, while serpentinized peridotite displays relatively flat patterns (Figure 9f) with LREE depletion ((La/Yb)N = 0.54), typical of refractory mantle. Low (Ce/Yb)N

Aceh Int. J. Sci. Technol., 14(1) 23-42
April 2025
doi: 10.13170/aijst.14.1.45308

ratios (0.48-2.43) and La/Yb ratios (0.60-3.74) indicate that the magma originated from partial melting of spinel peridotite at depths less than 40-50 km in the upper mantle.

Discussion
Magma Source

Rock samples from the Gunung Badak complex exhibit varying magma source characteristics. Diorite and basalt have Nb/La ratios <0.5 (ranging 0.23-0.44), indicating magma derived from lithospheric mantle sources (Hofmann, 1997) modified by subduction processes. Moderate Mg# values (49.67-58.13) in these rocks indicate that the magma has undergone moderate differentiation and is not primitive magma (Mg# >65). Based on Mg# values and SiO_2 content (50.69-52.52 wt%), diorite-basalt originated from the same parent magma that underwent crystal fractionation processes.

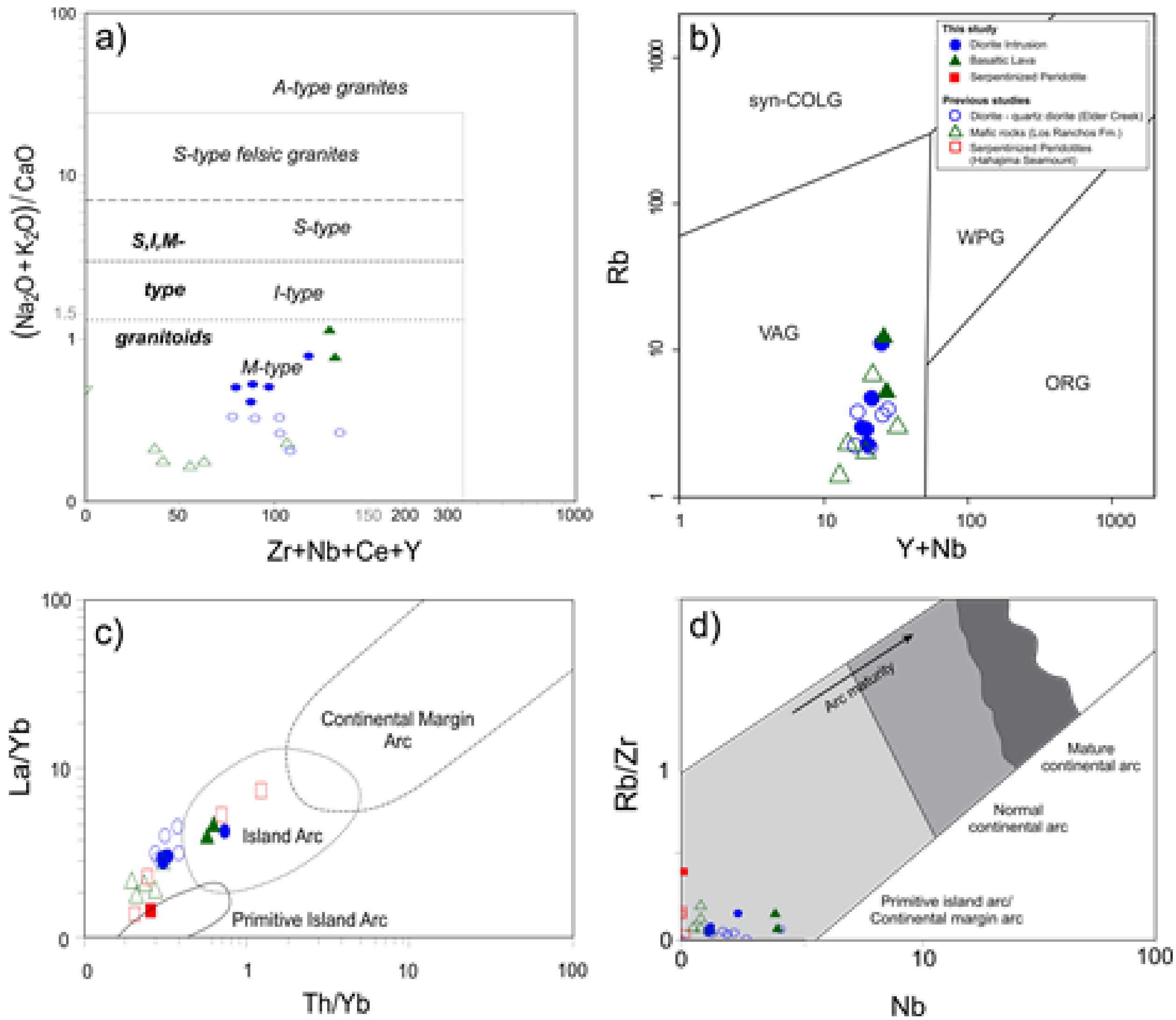

Figure 7. Tectono-magmatic discrimination diagrams of Gunung Badak Complex rocks. (a) (Na_2O+K_2O/CaO) vs. Zr+Nb+Ce+Y diagram (Whalen *et al.*, 1987). (b) Rb vs. Y+Nb diagram (Pearce *et al.*, 1984). (c) La/Yb vs. Th/Yb diagram (Condie, 1989). (d) Rb/Zr vs. Nb diagram (Brown *et al.*, 1984). Abbreviations: VAG = volcanic arc granites; ORG = ocean ridge granites; WPG = within-plates granites; syn-COLG = syn-collisional granites

doi: 10.13170/aijst.14.1.45308

High LILE/HFSE ratios and negative Nb-Ta anomalies in diorite-basalt demonstrate characteristics of derivative magma formed from metasomatized mantle due to fluid influence from the subducted plate (Li, 1992; Li *et al.*, 2013). High La/Nb ratios (2.21-3.75) and relatively low Th/La ratios (0.12-0.30) provide evidence that the magma originated from lithospheric mantle modified by subduction components (Condie, 1999).

Meanwhile, serpentinized peridotite exhibits exceptionally high Mg# (89.29) with subdued SiO_2 (40.59 wt%), characteristic of primitive upper mantle-derived material. Flat REE patterns with LREE depletion ($(La/Yb)_N$ = 0.54) indicate a highly depleted mantle source, possibly residual harzburgite that has undergone high-degree basaltic magma extraction (>30%) within a supra-subduction setting (Marchesi *et al.*, 2009). This rock is not part of the same magma series as diorite-basalt, but rather represents exhumed mantle fragments during tectonic processes.

Magma Evolution

Magma compositional changes are primarily caused by cooling processes, resulting in mineral crystallization from the liquid portion of magma, a process known as Fractional Crystallization (FC). Additionally, contamination is an important factor in magma differentiation. This contamination can occur through several mechanisms, including wall rock assimilation, mixing between two or more magma types, or even replenishment of magma chambers with juvenile, higher-temperature magma. These mechanisms contribute significantly to the compositional changes of the resulting magma (Etemadi *et al.*, 2019).

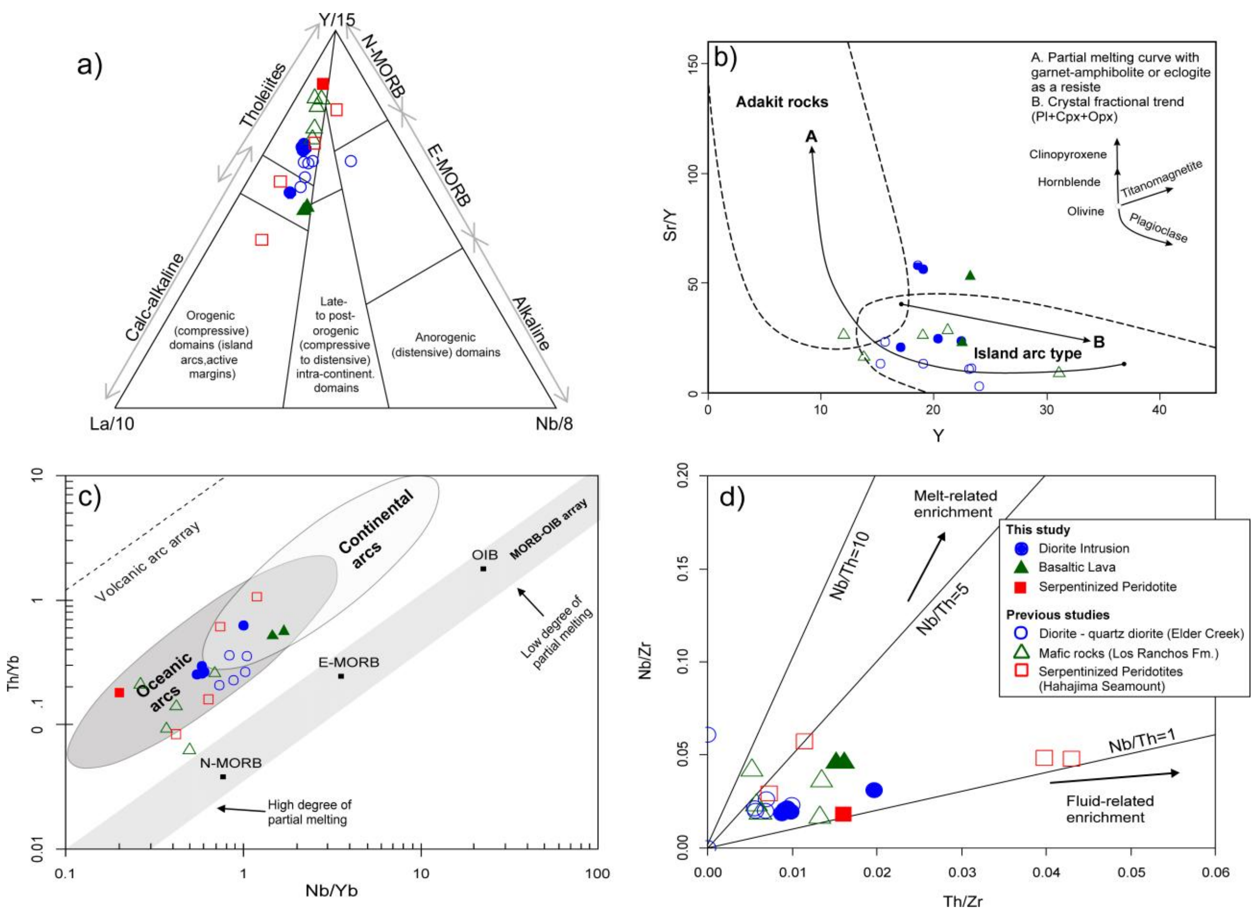

Figure 8. Tectonic discrimination diagrams of Gunung Badak Complex rocks (a) Y/15-La/10-Nb/8 (Cabanis and Lecolle, 1989); (b) Sr/Y vs. Y (Defant and Drummond, 1990); (c) Th/Yb vs. Nb/Yb (Pearce, 2014); (d) Nb/Zr vs. Th/Zr (Zhao and Zhou, 2007).

Partial melting and crystal fractionation constitute two fundamental mechanisms in magmatic processes and evolution (Li *et al*., 2020). The La/Sm versus La diagram (Figure 10b) demonstrates that fractional crystallization represents the dominant factor influencing magma evolution, while the V/Co vs. La/Sm plot (Figure 10c) indicates that diorite-basalt evolution exhibits a strong fractional crystallization (FC) signature. Conversely, serpentinized peridotite displays greater compatibility with mixing trends, although its proximity to the source region reflects limited mixing influence.

The La/Sm vs. La diagram (Figure 10b) illustrates that diorite-basalt follows a distinct fractional crystallization trend, with a positive linear correlation between La/Sm and La reflecting progressive accumulation of incompatible elements during mafic mineral fractionation (Li *et al*., 2020). Petrographic evidence for fractional crystallization processes is clearly observed in the porphyritic textures throughout all diorite-basalt samples, with variations in phenocryst size and abundance reflecting different differentiation stages (Marchesi *et al*., 2009).

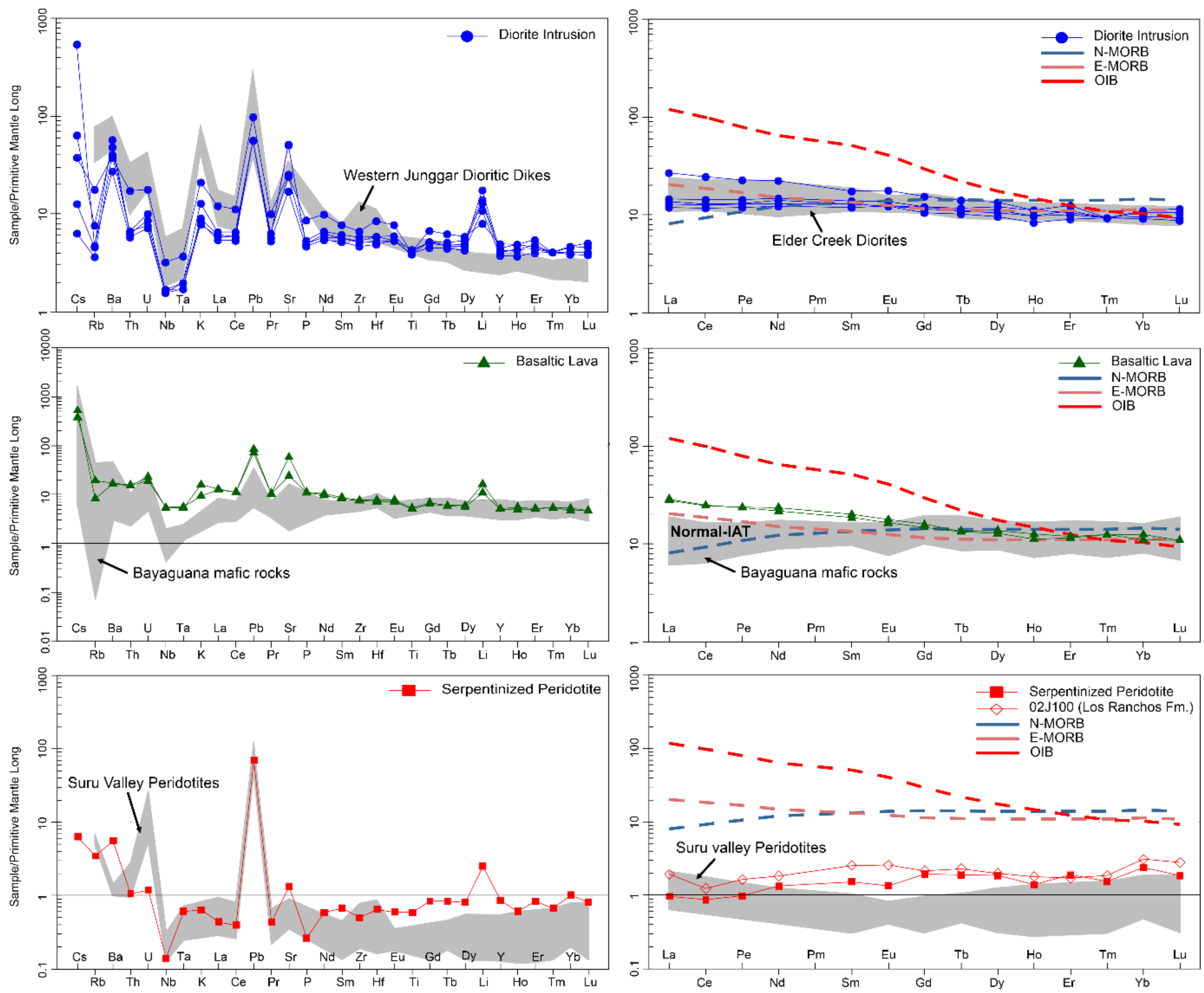

Figure 9. Trace element and REE distribution patterns normalized to primitive mantle and chondrite values, respectively. N-MORB, E-MORB, and OIB reference data from (Sun and McDonough, 1989). Comparative datasets incorporated from (Bhat *et al*., 2019; Escuder Viruete *et al*., 2006; Shervais, 2008; Torró *et al*., 2017; Yin *et al*., 2010).

The positioning of serpentinized peridotite far from the diorite-basalt fractional crystallization trend and its tendency toward mixing in the V/Co vs. La/Sm diagram (Figure 10c) confirms that serpentinized peridotite does not represent cumulates from the same magma but constitutes residual mantle material (Marchesi *et al*.,

doi: 10.13170/aijst.14.1.45308

2009). This trend is consistent with the petrographic textures of peridotite exhibiting mantle-like deformation characteristics such as kink bands, dynamic recrystallization, and exsolution lamellae in pyroxene, features that would not develop in magmatic cumulates (Chen *et al.*, 2023).

La/Yb ratios vary between 0.60-3.74, while Dy/Yb ratios display a limited range between 1.20-1.91 (Figure 10e). This reflects partial melting of a shallow source derived from spinel peridotite (Thirlwall *et al.*, 1994), indicating that garnet was not present as a residual phase in the source region and that the magma formed originated from depths less than 40 km (Haschke *et al.*, 2002; Kay *et al.*, 1991).

Diorite samples identified as spinel lherzolite exhibit partial melting degrees of 3-9%, while basalt associated with spinel lherzolite demonstrates partial melting of approximately 3%, and serpentinized peridotite in spinel lherzolite shows partial melting exceeding 30% (Figure 10f). Diorite and basalt display low to moderate LREE enrichment, whereas serpentinized peridotite exhibits LREE depletion, with relatively flat HREE patterns across all samples. These patterns indicate that the source rocks originated from shallow mantle composed of spinel lherzolite at depths less than 50 km (Murphy, 2007), in contrast to deeper mantle consisting of garnet lherzolite.

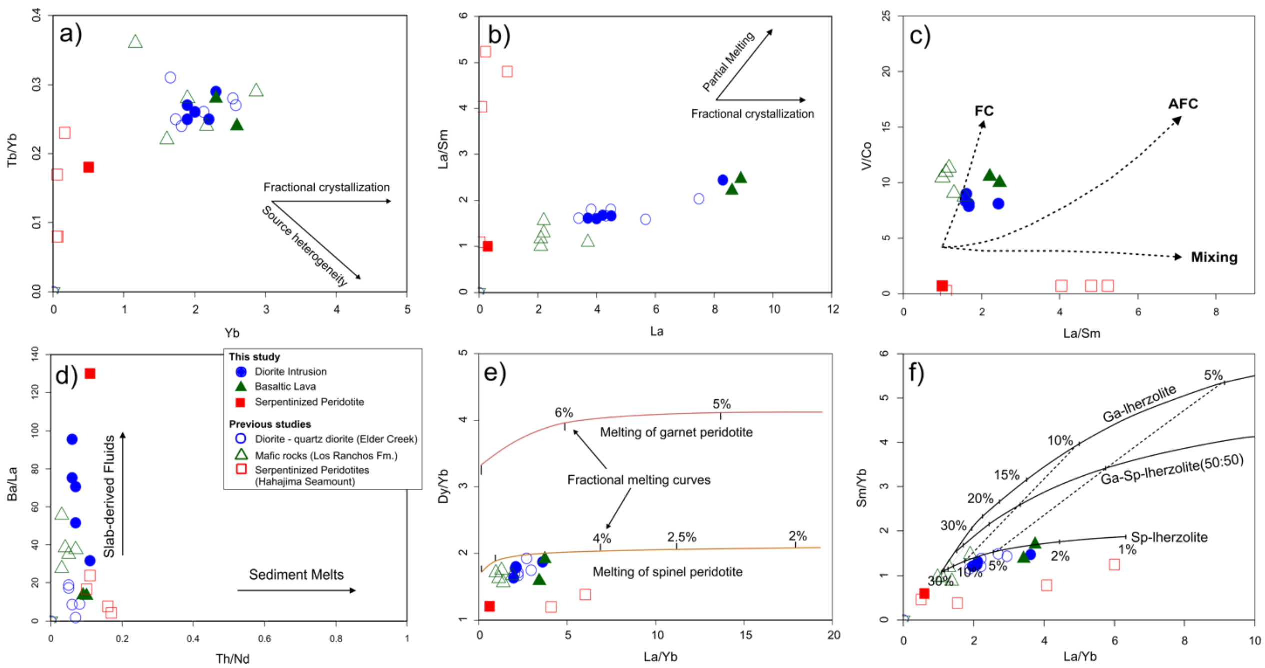

Figure 10. Discriminant plots: (a) Tb/Yb vs. Yb (Fan *et al.*, 2004); (b) La/Sm vs. La (Allègre and Minster, 1978); (c) V/Co vs. La/Sm (Etemadi *et al.*, 2019); (d) Ba/la vs. Th/Nd (Shaw, 1970); (e) Dy/Yb vs. La/Yb (Jung *et al.*, 2006); (f) Sm/Yb vs. La/Yb (Zhao and Zhou, 2009).

Tectonic Implication

The geochemical characteristics of igneous rocks from the Gunung Badak Complex provide important insights regarding their tectonic setting of formation (Figure 11). Determination through several tectonic discrimination diagrams yields interpretations related to geodynamic environments. In the Th/Yb vs. Nb/Yb diagram (Figure 8c), all rock samples consistently plot above the N-MORB/OIB array, a typical characteristic of magmatic rocks formed in subduction arc environments. The enrichment of Th relative to Nb in this ratio indicates a significant contribution of subduction components in magma petrogenesis.

Rocks of the Gunung Badak complex from the early Miocene demonstrate characteristic geochemistry of magmatic arcs. Based on the Rb vs. Y+Nb diagram (Figure 7b), all samples plot within the volcanic arc granite (VAG) field. Additionally, in the La/Yb vs. Th/Yb diagram (Figure 7c), these samples occur around the island arc field, generally categorized as calcic and metaluminous granitoids (Figure 5c) of M-type (Brown *et al.*, 1984). Generally, granites can be classified into I, S, M, and A types based on chemical composition and protolith characteristics (Whalen *et al*., 1987). Sample plots on the $(K_2O+Na_2O)/CaO$ vs. Zr+Nb+Ce+Y diagram (Figure 7a) also indicate that these samples belong to M-type.

Low K_2O and Rb contents in diorite-basalt rocks indicate that these rocks formed during the early stages of subduction processes, specifically in immature or early developmental stage island arcs (Maurice *et al*., 2013; Saito *et al*., 2004). Similarly, serpentinized peridotite also formed during early subduction stages but experienced rifting due to rollback, termed proto-arc (Satyana *et al*., 2021). This aligns with the sample positions plotting in the field of low maturity elements (Figure 7d). Conversely, relatively high K_2O and Rb contents would indicate rock formation in zones with thicker crust, possibly after the collision stage.

Geodynamic model

The Tb/Yb vs. Yb diagram (Figure 10a) displays a linear trend indicating fractional crystallization processes (FC) (Fan *et al*., 2004). Analysis of all samples demonstrates a linear trend indicating that these rocks formed from magma that underwent significant partial melting (Figure 10b). La/Yb ratios in rocks of the Gunung Badak Complex range from 0.6 to 3.74 (Faisal *et al*., 2020), indicating the absence of garnet as a residual phase in the source area. This suggests that magma formed at depths less than 50 km, considering that garnet is typically stable at depths exceeding 45-50 km (Nadermezerji *et al*., 2018).

The analyzed samples also contain relatively high HREE content (Yb 0.5-2.6 ppm, mostly >1.9 ppm) with flat HREE patterns (GdN/YbN = 1.03-1.47). These patterns indicate the presence of a spinel stability field in the magma source region. Additionally, low Dy/Yb ratios (1.2-1.92) further support the presence of a spinel stability field, as partial melts within the spinel stability field typically exhibit low Dy/Yb ratios (<1.5), whereas partial melts within the garnet stability field display high Dy/Yb ratios (>2.5) (Duggen *et al*., 2005; Yang *et al*., 2014). Based on these data, the rocks of the Gunung Badak Complex were most likely generated from partial melting of young mafic crust in a water-rich environment within the spinel stability field. This is supported by Th/Yb vs. Ta/Yb (Figure 8c), Nb/Zr vs. Th/Zr (Figure 8d), and Ba/La vs. Th/Nd (Figure 10d) diagrams, which demonstrate the influence of subduction fluids, magma derivation from metasomatized mantle, and characteristics of oceanic island arcs with parent magma formed through partial melting of a depleted mantle source.

Conclusions

Based on the analysis and interpretation of the data conducted, this study concludes that:

1. Ultramafic rocks in the form of serpentinized peridotite in the Gunung Badak Complex exhibit geochemical affinities IAT (Island Arc Tholeiitic), characterizing a supra-subduction zone (SSZ) environment, with LREE depletion indicating derivation from lithospheric mantle metasomatized by subduction fluids.
2. Intermediate and mafic rocks (diorite and basalt) exhibit tholeiitic series with low-K (tholeiitic) content formed in an immature island arc environment during the Early Miocene (~22 Ma), characterized by LILE enrichment relative to HFSE and distinct negative Nb-Ta anomalies.
3. Trace element and rare earth element (REE) patterns indicate that rocks of the Gunung Badak Complex originated from two distinct magmatic episodes including exhumation of mantle peridotite during Eocene subduction initiation processes, and intermediate-mafic arc magmatism during Early Miocene arc development.
4. Further studies involving absolute age determination through K-Ar dating of diorite and serpentinized peridotite, Sr-Nd-Pb isotope analysis, and thermobarometry of rocks from the Gunung Badak Complex are necessary to clarify magmatism chronology, characterize magma sources, and reconstruct rock formation conditions.

Acknowledgement

The authors are grateful to the Beasiswa Unggulan Program of the Ministry of Education, Culture, Research, and Technology (Kemendikbudristek) for educational funding support, Padjadjaran University for financing this research through the Academic Leadership Grant (ALG) scheme, as well as to the UNESCO Ciletuh-Palabuhanratu Global Geopark Management Authority and all colleagues who provided assistance during the fieldwork and research Tableprocess.

doi: 10.13170/aijst.14.1.45308

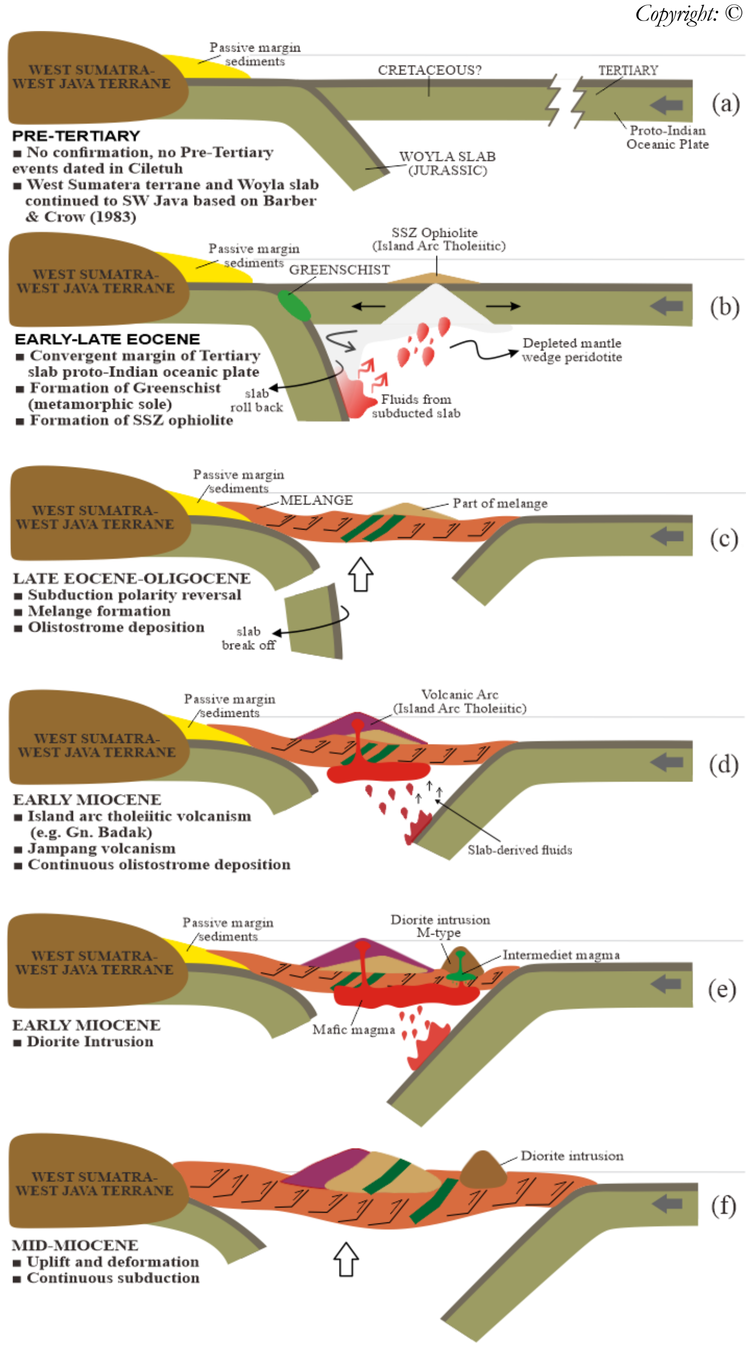

Figure 11. Schematic sequential tectonic model illustrating intra-oceanic magmatic evolution in the Gunung Badak Complex, Ciletuh (modified from Satyana *et al.*, 2021). **(a)** In the early stage (Pre-Tertiary), no evidence of tectonic activity is found in Ciletuh. This region represents a passive margin without significant activity. However, the West Sumatra Terrane and Woyla plate are estimated to extend to southwestern Java (Barber and Crow, 1983). **(b)** The presence of SSZ (Supra-Subduction Zone) ophiolite in Ciletuh, geochemically characterized by island arc tholeiitic signatures, indicates that petrogenesis occurred due to subduction rollback of an old oceanic slab, causing rifting in the overriding plate. **(c)** Mélange formed after ophiolite metamorphic processes and petrogenesis, involving sediments from the continental margin and subduction plate segments. Reverse subduction occurring from late Eocene to Oligocene progressed alongside mélange formation and thrusting. **(d)** During the Early Miocene period, island arc tholeiitic (IAT) volcanic activity resumed, producing basaltic lava as found in Gunung Badak. This volcanism occurred in a subduction zone active since the Eocene period, generating basaltic pillow lavas. **(e)** In the southern part of Gunung Badak, magmatic intrusion formed diorite rocks, indicating continued magmatism related to subduction development in the upper Early Miocene stage. **(f)** The region experienced uplift, deformation, and continued subduction during the Middle Miocene to subsequent periods, forming increasingly complex geological structures.

References

Ahmed, A.H., Arai, S., Abdel-aziz, Y.M., and Rahimi, A. 2005. Spinel Composition as a Petrogenetic Indicator of The Mantle Section in The Neoproterozoic Bou Azzer Ophiolite, Anti-Atlas, Morocco. *Precambrian Research*, 138, 225–234. https://doi.org/10.1016/j.precamres.2005.05.004

Allègre, C.J. and Minster, J.F. 1978. Quantitative Models of Trace Element Behavior in Magmatic Processes. *Earth and Planetary Science Letters*, 38, 1–25. https://doi.org/10.1016/0012-821X(78)90123-1

Barret, T.J. and MacLean, W.H. 1994. Chemostratigraphy and Hydrothermal Alteration in Exploration for VHMS Deposits in Greenstone and Younger Volcanic Rocks, Short Course Notes. Geological Association of Canada. https://gq.mines.gouv.qc.ca/documents/EXAMINE/GM60861/GM60861.pdf

Bhat, I.M., Ahmad, T., and Subba Rao, D.V. 2019. Origin and Evolution of Suru Valley Ophiolite Peridotite Slice along Indus Suture Zone, Ladakh Himalaya, India: Implications on Melt-rock Interaction in a Subduction-Zone Environment. *Geochemistry*, 79, 78–93. https://doi.org/10.1016/j.chemer.2018.10.003

Brown, G.C., Thorpe, R.S., and Webb, P.C. 1984. The Geochemical Characteristics of Granitoids in Contrasting Arcs and Comments on Magma Sources. Journal of The Geological Society, 141, 413–426. https://doi.org/10.1144/gsjgs.141.3.0413

Cabanis, B. and Lecolle, M., 1989. The La/10-Y/15-Nb/8 diagram: A tool for distinguishing volcanic series and discovering crustal mixing and/or contamination. Comptes Rendus Acad. Sci. Série 2 309, 20.

Chen, K., Tang, M., Hu, Z., and Liu, Y. 2023. Generation of Tholeiitic and Calc-alkaline Arc Magmas and Its Implications for Continental Growth. *Geochimica et Cosmochimica Acta*, 355, 173–183. https://doi.org/10.1016/j.gca.2023.07.002

Coleman, R.G. 1977. Ophiolites: Ancient Oceanic Lithosphere?, Minerals and Rocks. Springer Berlin Heidelberg, Berlin, Heidelberg. https://doi.org/10.1007/978-3-642-66673-5

Condie, K.C. 1999. Mafic Crustal Xenoliths and The Origin of The Lower Continental Crust. *Lithos,* 46, 95–101. https://doi.org/10.1016/S0024-4937(98)00056-5

Condie, K.C., 1989. Geochemical Changes in Baslts and Andesites Across The Archean-Proterozoic Boundary: Identification and Significance. *Lithos*, 23, 1–18. https://doi.org/10.1016/0024-4937(89)90020-0

Defant, M.J. and Drummond, M.S. 1990. Derivation of Some Modern Arc Magmas by Melting of Young Subducted Lithosphere. *Nature*, 347, 662–665. https://doi.org/10.1038/347662a0

Duggen, S., Hoernle, K., Van Den Bogaard, P., and Garbe-Schönberg, D. 2005. Post-Collisional Transition from Subduction- to Intraplate-type Magmatism in The Westernmost Mediterranean: Evidence for Continental-Edge Delamination of Subcontinental Lithosphere. *Journal of Petrology,* 46, 1155–1201. https://doi.org/10.1093/petrology/egi013

Dupuis, C., Hébert, R., Dubois-Côté, V., Guilmette, C., Wang, C.S., Li, Y.L., and Li, Z.J. 2005. The Yarlung Zangbo Suture Zone Ophiolitic Mélange (Southern Tibet): New Insights from Geochemistry of Ultramafic Rocks. *Journal of Asian Earth Sciences*, 25, 937–960. https://doi.org/10.1016/j.jseaes.2004.09.004

Escuder Viruete, J., Díaz De Neira, A., Hernáiz Huerta, P.P., Monthel, J., Senz, J.G., Joubert, M., Lopera, E., Ullrich, T., Friedman, R., and Mortensen, J. 2006. Magmatic Relationships and Ages of Caribbean Island Arc Tholeiites, Boninites and Related Felsic Rocks, Dominican Republic. *Lithos* 90, 161–186. https://doi.org/10.1016/j.lithos.2006.02.001

Etemadi, A., Karimpour, M.H., Shafaroudi, A.M., Santos, J.F., Mathur, R., and Ribeiro, S. 2019. U-Pb Zircon Geochronology, Geochemistry, and Petrogenesis of The Hamech Intrusions in The Kuh-e-Shah Volcano-Plutonic Complex, Eastern Iran. *Turkish Journal of Earth Science*, 28, 38–59. https://doi.org/10.3906/yer-1710-5

Faisal, M., Yang, X., Khalifa, I.H., Amuda, A.K., and Sun, C. 2020. Geochronology and Geochemistry of Neoproterozoic Hamamid Metavolcanics Hosting Largest Volcanogenic Massive Sulfide Deposits in Eastern Desert of Egypt: Implications for Petrogenesis and Tectonic Evolution. *Precambrian Research* 344, 105751. https://doi.org/10.1016/j.precamres.2020.105751

Fan, W.-M., Guo, F., Wang, Y.-J., and Zhang, M. 2004. Late Mesozoic Volcanism in The Northern Huaiyang Tectono-magmatic Belt, Central China: Partial Melts from a Lithospheric Mantle with Subducted Continental Crust Relicts Beneath The Dabie Orogen?. *Chemical Geology*, 209, 27–48. https://doi.org/10.1016/j.chemgeo.2004.04.020

Gill, J.B. 1981. Orogenic Andesites and Plate Tectonics, Minerals and Rocks. Springer Berlin Heidelberg, Berlin, Heidelberg. https://doi.org/10.1007/978-3-642-68012-0

Gill, R. 2010. Igneous Rocks and Processes: A Practical Guide. Wiley. https://zarmesh.com/wp-content/uploads/2018/08/Igneous_Rocks_and_Processes.pdf

Green, N.L. 2006. Influence of Slab Thermal Structure on Basalt Source Regions and Melting Conditions: REE and HFSE Constraints from The Garibaldi Volcanic Belt, Northern Cascadia Subduction System. *Lithos,* 87, 23–49. https://doi.org/10.1016/j.lithos.2005.05.003

Gu, X., Deloule, E., France, L., and Ingrin, J. 2016. Multi-stage Metasomatism Revealed by Trace Element and Li isotope Distributions in Minerals of Peridotite Xenoliths from Allègre Volcano (French Massif Central). *Lithos*, 264, 158–174. https://doi.org/10.1016/j.lithos.2016.07.019

Hall, R., Clements, B., Smyth, H.R., and Cottam, M.A. 2007. A New Interpretation of Java's Structure, in: *Proceedings Indonesian Petrolleum Association, 31st Annual Convention Presented at the Thirty-First Annual Convention, Indonesian Petroleum Association (IPA)*. https://doi.org/10.29118/IPA.1077.07.G.035

Hamilton, W.B. 1979. Tectonics of The Indonesian Region. U.S. Geological Survey Professional Paper, 1078. https://doi.org/10.3133/pp1078

Hardiyono, A., Ikhram, R., Haq, H.N., Rosana, M.F., Syafri, I., Yuningsih, E.T., Mufti, M., and Permana, H. 2022. New Consideration of Origin of The Gunung Badak Basaltic Lava, Ciletuh Area, Indonesia. Journal of *Engineering Science and Technology* Special Issue 4/2023, 1–7. https://jestec.taylors.edu.my/Special%20Issue%20AASEC2022/RPI_SI_2023_1.pdf

Harker, A., 1909. The Natural History of Igneous Rocks. Methuen & Company, London, UK. https://scispace.com/pdf/the-natural-history-of-igneous-rocks-1qoan89q5f.pdf

Haschke, M., Siebel, W., Günther, A., and Scheuber, E. 2002. Repeated Crustal Thickening and Recycling During The Andean Orogeny in North Chile (21°–26°S). *Journal Geophysical Research: Solid Earth*, 107. https://doi.org/10.1029/2001JB000328

Hellebrand, E., Snow, J.E., and Mühe, R. 2002. Mantle Melting Beneath Gakkel Ridge (Arctic Ocean): Abyssal Peridotite Spinel Compositions. *Chemical Geology*, 182, 227–235. https://doi.org/10.1016/S0009-2541(01)00291-1

Hofmann, A.W. 1997. Mantle Geochemistry: The Message from Oceanic Volcanism. *Nature,* 385, 219–229. https://doi.org/10.1038/385219a0

Ikhram, R., Syafri, I., and Rosana, M.F. 2023. Petrology, Geochemistry and K-Ar Dating of Metamorphic Rock in Ciletuh Mélange Complex, West Java Indonesia. *Riset Geologi dan Pertambangan*, 33. https://doi.org/10.55981/risetgeotam.2023.1054

Irvine, T.N. and Baragar, W.R.A. 1971. A Guide to The Chemical Classification of The Common Volcanic Rocks. Canadian Journal of Earth Science, 8, 523–548. https://doi.org/10.1139/e71-055

Jung, C., Jung, S., Hoffer, E., and Berndt, J. 2006. Petrogenesis of Tertiary Mafic Alkaline Magmas in The Hocheifel, Germany. *Journal of Petrology*, 47, 1637–1671. https://doi.org/10.1093/petrology/egl023

Katili, J.A. 1975. Volcanism and Plate Tectonics in The Indonesian Island Arcs. *Tectonophysics*, 26, 165–188. https://doi.org/10.1016/0040-1951(75)90088-8

Kay, S.M., Mpodozis, C., Ramos, V.A., and Munizaga, F. 1991. Magma Source Variations for Mid–late Tertiary Magmatic Rocks Associated with a Shallowing Subduction Zone and a Thickening Crust in The Central Andes (28 to 33°S). Geological Society of America, pp. 113–138. https://doi.org/10.1130/SPE265-p113

Le Maitre, R.W., Bateman, P., Dudek, A., Keller, J., Lameyre, J., Le Bas, M.J., Sabine, P.A., Schmid, R., Sorensen, H., Streckeisen, A., Woolley, A.R., and Zanettin, B. 1989. A Classification of Igneous Rocks and Glossary of Terms. Blackwell Scientific Publications, Oxford. https://archive.org/details/classificationof0000inte

Li, C.N. 1992. Trace Element Petrology of Igneous Rocks. China University of Geosciences Press, Wuhan, China.

Li, P., Yu, X., Li, H., Qiu, J., and Zhou, X. 2013. Jurassic–Cretaceous Tectonic Evolution of Southeast China: Geochronological and Geochemical Constraints of Yanshanian Granitoids. *International Geology Review,* 55, 1202–1219. https://doi.org/10.1080/00206814.2013.771952

Li, T., Liu, L., Liao, X.-Y., Gai, Y.-S., Ma, T., and Wang, C. 2020. Geochemistry, Sr-Nd-Pb Isotopic Compositions and Zircon U-Pb Geochronology of Neoproterozoic Mafic Dyke in the Douling Complex, South Qinling Belt, China. *Journal of Earth Science*, 31, 237–248. https://doi.org/10.1007/s12583-020-1298-6

Marchesi, C., Garrido, C.J., Godard, M., Belley, F., and Ferré, E. 2009. Migration and Accumulation of Ultra-Depleted Subduction-related Melts in The Massif du Sud ophiolite (New Caledonia). *Chemical Geology*, 266, 171–186. https://doi.org/10.1016/j.chemgeo.2009.06.004

Martodjojo, A., Suparka, A., and Hadiwisastra, S., 1977. Status formasi Ciletuh dalam evolusi Jawa Barat. Ikatan Ahli Geologi Indonesia.

Maurice, A.E., Bakhit, B.R., Basta, F.F., and Khiamy, A.A. 2013. Geochemistry of Gabbros and Granitoids (M- and I-types) from The Nubian Shield of Egypt: Roots of Neoproterozoic Intra-oceanic Ssland arc. *Precambrian Research*, 224, 397–411. https://doi.org/10.1016/j.precamres.2012.10.012

Mercier, J.-C.C. and Nicolas, A. 1975. Textures and Fabrics of Upper-Mantle Peridotites as Illustrated by Xenoliths from Basalts. *Journal of Petrology*, 16, 454–487. https://doi.org/10.1093/petrology/16.1.454

Middlemost, E.A.K. 1994. Naming Materials in The Magma/igneous Rock System. *Earth-Science Reviews*, 37, 215–224. https://doi.org/10.1016/0012-8252(94)90029-9

Murphy, J.B. 2007. Igneous Rock Associations 8. Arc Magmatism II: Geochemical and Isotopic Characteristics. *Geoscience Canada*, 34, 7–35. https://www.erudit.org/en/journals/geocan/2007-v34-n1-geocan_34_1/geocan34_1ser01.pdf

Nadermezerji, S., Karimpour, M.H., Shafaroudi, A.M., Santos, J.F., Mathur, R., and Ribeiro, S. 2018. U–Pb Geochronology, Sr–Nd Isotopic Compositions, Geochemistry and Petrogenesis of Shah Soltan Ali Granitoids, Birjand, Eastern Iran. *Geochemistry*, 78, 299–313. https://doi.org/10.1016/j.chemer.2018.08.003

Pearce, J.A. 2014. Immobile Element Fingerprinting of Ophiolites. *Elements*, 10, 101–108. https://doi.org/10.2113/gselements.10.2.101

Pearce, J.A., Harris, N.B.W., and Tindle, A.G., 1984. Trace Element Discrimination Diagrams for The Tectonic Interpretation of Granitic Rocks. *Journal of Petrology,* 25, 956–983. https://doi.org/10.1093/petrology/25.4.956

Pfeifer, H.R. 1979. Fluid-Gesteins-Interaktion in Metamorphen Ultramafititen der Zentralalpen (Doctoral dissertation). ETH Zurich, Zurich. https://www.research-collection.ethz.ch/bitstream/handle/20.500.11850/136730/eth-35132-01.pdf?sequence=1

Rosana, M.F., Isnaniawardhani, V., Hardiyono, A., Helmi, F., Brilian, C.H., Nugraha, K.S.A., and Faturrakhman, M.L. 2019. Peta geologi lembar Cikadal-Lengkong (1208-43) dan (1208-64), Jawa Barat, skala 1: 50.000.

Saha, A., Santosh, M., Ganguly, S., Manikyamba, C., Ray, J., and Dutta, J. 2018. Geochemical Cycling During Subduction Initiation: Evidence from Serpentinized Mantle Wedge Peridotite in The South Andaman Ophiolite Suite. *Geoscience Frontiers*, 9, 1755–1775. https://doi.org/10.1016/j.gsf.2017.12.017

Saito, S., Arima, M., Nakajima, T., and Kimura, J.-I. 2004. Petrogenesis of Ashigawa and Tonogi Granitic Intrusions, Southern Part of The Miocene Kofu Granitic Complex, Central Japan: M-type Granite in The Izu Arc Collision Zone. *Journal of Mineralogical and Petrological Sciences*, 99, 104–117. https://doi.org/10.2465/jmps.99.104

Satyana, A.H., Prasetyo, A., Rosana, M.F., 2021. Ciletuh Subduction, West Java - New Findings, New Problems: Regional Implications to Cretaceous-Paleogene Convergence of Sundaland Margin and Its Petroleum Geology, in: Proc of the Indonesian Petroleum Association 44th Annual Convention and Exhibition. Presented at the Indonesian Petroleum Association 44th Annual Convention and Exhibition, Indonesian Petroleum Association. https://doi.org/10.29118/IPA21-G-29

Satyana, A.H., Prasetyo, A., and Rosana, M.F. 2021. Ciletuh Subduction, Southwest Java-New Findings: Nature, Age, and Regional Implications. Proceedings, Indonesian Petroleum Association. https://geologi.fitb.itb.ac.id/wp-content/uploads/sites/63/2021/09/IPA21-G-29.pdf

Shand, S.J. 1943. Eruptive Rocks: Their Genesis, Composition, Classification, and Their Relation to Ore-deposits, with a Chapter on Meteorites. John Wiley & Sons, inc. New York. https://archive.org/details/bwb_KS-371-745

Shaw, D.M. 1970. Trace Element Fractionation During Anatexis. *Geochimica et Cosmochimica Acta*, 34, 237–243. https://doi.org/10.1016/0016-7037(70)90009-8

Shervais, J.W., 2008. Tonalites, Trondhjemites, and Diorites of The Elder Creek Ophiolite, California: Low-pressure Slab Melting and Reaction with The Mantle Wedge. in: Special Paper 438: Ophiolites, Arcs, and Batholiths: A Tribute to Cliff Hopson. Geological Society of America, pp. 113–132. https://doi.org/10.1130/2008.2438(03)

Sukamto, R. 1975. Peta geologi lembar Jampang dan Balekambang, Jawa. Skala 1: 100000.

Sun, S. -s. and McDonough, W.F. 1989. Chemical and Isotopic Systematics of Oceanic Basalts: Implications for Mantle Composition and Processes. SP 42, 313–345. https://doi.org/10.1144/GSL.SP.1989.042.01.19

Thayyib, E.S., Said, E.L., Siswoyo, and Prijomarsono, S. 1977. The Status of The Melange Complex in Ciletuh Area, South-West Java. *Proceedings Indonesian Petroleum Association*, Sixth Annual Convention 241–253. https://geologi.fitb.itb.ac.id/wp-content/uploads/sites/63/2021/09/241.pdf

Thirlwall, M.F., Upton, B.G.J., and Jenkins, C. 1994. Interaction Between Continental Lithosphere and The Iceland Plume--Sr-Nd-Pb Isotope Geochemistry of Tertiary Basalts, NE Greenland. *Journal of Petrology,* 35, 839–879. https://doi.org/10.1093/petrology/35.3.839

Torró, L., Camprubí, A., Proenza, J.A., León, P., Stein, H.J., Lewis, J.F., Nelson, C.E., Chavez, C., and Melgarejo, J.C. 2017. Re-Os and U-Pb Geochronology of The Doña Amanda and Cerro Kiosko Deposits, Bayaguana District, Dominican Republic: Looking Down for The Porphyry Cu-Mo Roots of the Pueblo Viejo-Type Mineralization in the Island-Arc Tholeiitic Series of the Caribbean. *Economic Geology*, 112, 829–853. https://doi.org/10.2113/econgeo.112.4.829

Van Bemmelen, R.W. 1949. The Geology of Indonesia Vol. IA, The Geology of Indonesia of Indonesia and Adjacent Archipelagoes. Government Printing Office, The Hague. https://langka.lib.ugm.ac.id/viewer/index/1461

Verbeek, R.D.M. and Fennema, R., 1896. Geologische beschrijving van Java en Madura. Amsterdam. https://catalog.hathitrust.org/Record/006178891

Whalen, J.B., Currie, K.L., and Chappell, B.W. 1987. A-type granites: Geochemical Characteristics, Discrimination and Petrogenesis. *Contributions to Mineral and Petrology*, 95, 407–419. https://doi.org/10.1007/BF00402202

Wilson, M. 1989. Igneous Petrogenesis a Global Tectonic Approach. Springer Netherlands, Dordrecht. https://doi.org/10.1007/978-1-4020-6788-4

Wu, T., Tian, L., Gao, J., and Dong, Y. 2019. Petrology and Geochemistry of Serpentinized Peridotites from Hahajima Seamount in Izu-Bonin Forearc Region. *Acta Oceanologica Sinica,* 38, 99–110. https://doi.org/10.1007/s13131-019-1469-x

Yang, Q., Santosh, M., Shen, J., and Li, S. 2014. Juvenile vs. Recycled Crust in NE China: Zircon U–Pb Geochronology, Hf Isotope and an Integrated Model for Mesozoic Gold Mineralization in The Jiaodong Peninsula. *Gondwana Research*, 25, 1445–1468. https://doi.org/10.1016/j.gr.2013.06.003

Yin, J., Yuan, C., Sun, M., Long, X., Zhao, G., Wong, K.P., Geng, H., and Cai, K. 2010. Late Carboniferous high-Mg Dioritic Dikes in Western Junggar, NW China: Geochemical Features, Petrogenesis and Tectonic Implications. *Gondwana Research*, 17, 145–152. https://doi.org/10.1016/j.gr.2009.05.011

Zhao, J., Long, X., Dong, Y., Li, J., Gao, Y., and Zhao, B. 2019. Petrogenesis, Tectonic Setting and Formation Age of The Metaperidotites in The Lajishan Ophiolite, Central Qilian Block, NW China. *Journal of Asian Earth Sciences*, 186, 104076. https://doi.org/10.1016/j.jseaes.2019.104076

Zhao, J.-H. and Zhou, M.-F. 2009. Secular Evolution of The Neoproterozoic Lithospheric Mantle Underneath The Northern Margin of The Yangtze Block, South China. *Lithos*, 107, 152–168. https://doi.org/10.1016/j.lithos.2008.09.017

Zhao, J.-H., and Zhou, M.-F. 2007. Geochemistry of Neoproterozoic Mafic Intrusions in The Panzhihua District (Sichuan Province, SW China): Implications for Subduction-related Metasomatism in The Upper Mantle. *Precambrian Research*, 152, 27–47. https://doi.org/10.1016/j.precamres.2006.09.002